Supporting Information for : Stable and high yield growth of GaP and $In_{0.2}Ga_{0.8}As$ nanowire arrays using In as a catalyst

Andrea Scaccabarozzi,[†,‡] Andrea Cattoni,[†] Gilles Patriarche,[†] Laurent Travers,[†] Stéphane Collin,[†] Jean-Christophe Harmand,[†] Frank Glas,[†] and Fabrice Oehler[*,†]

†*Université Paris-Saclay, CNRS, Centre de Nanosciences et de Nanotechnologies, 91120, Palaiseau, France*

‡*Institut Photovoltaïque d'Ile-de-France, 91120, Palaiseau, France*

E-mail: fabrice.oehler@c2n.upsaclay.fr

Thermodynamics

Equilibrium group V concentrations in the liquid droplet

Using standard equilibrium technique (SET), we solve for for each temperature (T) the full equilibrium solution and we obtain composition (x) of the solid $In_{1-x}Ga_xZ$ (Z=As,P), the full composition of the liquid (y_i, i=In,Ga,Z) for a given temperature T.

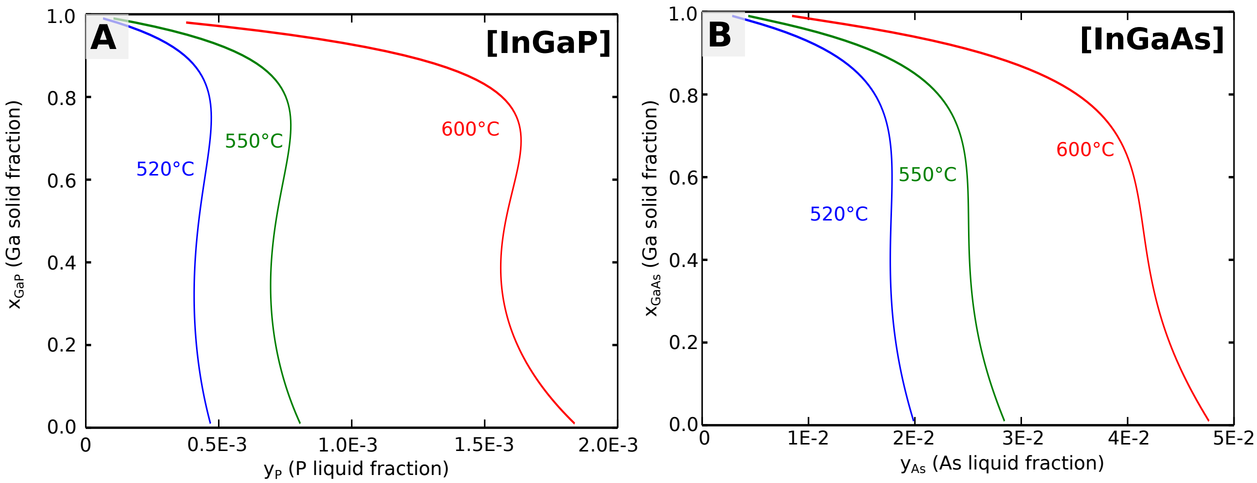

Figure S1: (a) Equilibrium fractions of P (y_P) in a [InGaP] liquid in contact with $\mathrm{In_{1-x}Ga_xP}$ solid at 520°C, 550°C and 660°C. (b) Similar results with the equilibrium fractions of As in a [InGaAs] liquid in contact with $\mathrm{In_{1-x}Ga_xAs}$ solid.

Figure S1 presents the results for $\mathrm{In_{1-x}Ga_xP}$ (Fig. S1.a) and $\mathrm{In_{1-x}Ga_xAs}$ (Fig. S1.b) solids in contact with [InGaAs] and [InGaP] liquids respectively.

For $\mathrm{In_{1-x}Ga_xP}$ the typical P content in the droplet is $y_P \simeq 10^{-3}$. For $\mathrm{In_{1-x}Ga_xAs}$, the As content in the [InGaAs] droplet (y_{As}) is typically one magnitude higher, $y_{As} \simeq 10^{-2}$.

Note that the relation between y_Z (Z=As,P) and x_{GaZ} is not simple due to the miscibility gaps in the InGaP (below 650°C)[1] and InGaAs (below 545°C)[2] solids.

In all cases, the group V concentration in the droplet determined by SET is at most a few percent atomic composition.

Reference thermodynamic data

In the regular solution framework, the chemical potential μ_i^p of the specie i in the liquid ($p = l$) or solid ($p = s$) phase is obtained from the reference chemical potential $\mu_i^{p\,0}$ and the mixing coefficient with the other components j ($j \neq i$). Theses mixing coefficients are usually noted as ω_{ij} in the liquid phase and Ω_{ij} in the solid phase.

To ease the calculation, we reproduce in Table ST1 the relevant literature data used in this study.

Table ST1: Reference thermodynamic data used in the SET and NT calculations, expressed in J.mol^{-1}, the temperature T is in Kelvin.

$\mu^{l\,0}_{Ga}$	$-1389.188 + 114.049043 \cdot T - 26.0692906 \cdot T \cdot \ln T + 0.1506\text{e-}3 \cdot T^2 - 0.040173\text{e-}6 \cdot T^3 - 118332 \cdot T^{-1}$	ref[3]
$\mu^{l\,0}_{In}$	$-3749.808 + 116.835756 \cdot T - 27.4562 \cdot T \cdot \ln T + 0.54607\text{e-}3 \cdot T^2 - 0.08367\text{e-}6 \cdot T^3 - 211708 \cdot T^{-1}$	ref[3]
$\mu^{l\,0}_{P}$	$-7232.449 + 133.291873 \cdot T - 26.326 \cdot T \cdot \ln T$	ref[3]
$\mu^{l\,0}_{As}$	$17172.453 + 99.78639 \cdot T - 23.3144 \cdot T \cdot \ln T - 2.71613\text{e-}3 \cdot T^2 + 11600 \cdot T^{-1}$	ref[3]
$0.5 \cdot \mu^{s\,0}_{GaAs}$	$-52176 + 132.71628 \cdot T - 24.340629 \cdot T \cdot \ln T - 0.0005579 \cdot T^2 + 63835.0 \cdot T^{-1} - 3.5689\text{e-}7 \cdot T^3$	ref[4]
$0.5 \cdot \mu^{s\,0}_{GaP}$	$-65760.76 + 142.37445 \cdot T - 24.7902 \cdot T \cdot \ln T - 0.7113\text{e-}3 \cdot T^2 + 146440 \cdot T^{-1}$	ref[4]
$0.5 \cdot \mu^{s\,0}_{InAs}$	$-36528.6 + 115.45948 * T - 22.593917 \cdot T \cdot \ln T - 0.003865 \cdot T^2 + 34719.0 \cdot T^{-1} + 7.09\text{e-}8 \cdot T^3$	ref[4]
$0.5 \cdot \mu^{s\,0}_{InP}$	$-47600.60 + 179.24993 \cdot T - 31.793476 \cdot T \cdot \ln T + 7.880317\text{e-}3 \cdot T^2 + 220897 \cdot T^{-1} - 1.81522\text{e-}6 \cdot T^3$	ref[4]
ω_{AsGa}	$-25503.6 - 4.3109 \cdot T + (c_{As} - c_{Ga}) \cdot (-5174.7)$	ref[4]
ω_{AsIn}	$-15851.0 - 11.27053 \cdot T + (c_{As} - c_{In}) \cdot (-1219.5)$	ref[4]
ω_{GaIn}	$4450.0 + 1.19185 \cdot T + (c_{Ga} - c_{In}) \cdot 0.25943 \cdot T$	ref[4]
ω_{GaP}	-9862	ref[4]
ω_{InP}	$14124.08 - 10.17931 \cdot T + (c_{In} - c_P) \cdot 2900.0$	ref[4]
$\Omega_{GaP-InP}$	$(17455.105 - 2.9062362 \cdot T) + (x_{GaP} - x_{InP}) * (1111.2757 + 1.0119981 \cdot T)$	ref[1]
$\Omega_{GaAs-InAs}$	$1.96988\text{e}4 - 7.51693 \cdot T$	ref[2]

Chemical composition of [In]-GaP nanowires grown using a high In flux (Ga:In = 1:4)

In addition to the main text, which shows the STEM-EDS analysis of [In]-(InGa)As and [In]-GaP NWs grown using Ga:In = 1:1 (Fig. 2, main text), Fig. S2 presents the STEM-EDS analysis of [In]-GaP NWs grown using Ga:In = 1:4. These NWs are used in the morphological comparison of the main text, when increasing the In flux from Ga:In = 1:0 to 1:4 (see Table 1, main text).

Despite the use of a higher In flux, Ga:In = 1:4 compared 1:1, the solid phase remains near pure GaP ($\mathrm{In_xGa_{(1-x)}P}$ with $x_{InP} = 0.01 \pm 0.01$) while the liquid composition is nearly pure In ($y_{In} = 0.96 \pm 0.01$, $y_{Ga} = 0.03 \pm 0.01$, $y_P = 0.01 \pm 0.01$). Within our standard EDS experimental error, the chemical composition of these [In]-GaP NWs with Ga:In = 1:4 is very close to that grown using Ga:In = 1:1.

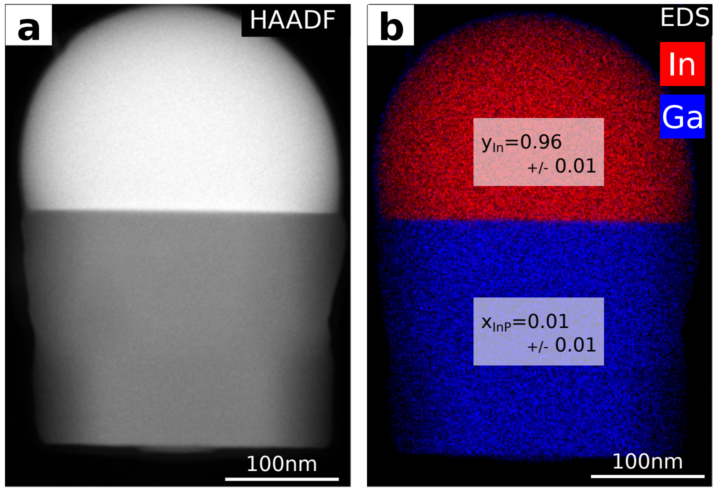

Figure S2: STEM-EDS analysis of [In]-GaP NWs grown using Ga:In = 1:4 flux ratio. The NWs are dispersed on a standard TEM grid. (a) STEM-HAAD image the NW. (b) Corresponding STEM-EDS elemental maps showing the In (red) and Ga (blue) composition. The In contents of the solid (x_{InP}) and liquid (y_{In}) phases are indicated.

Crystal phase of Ga-catalyzed GaP NWs

The apparition of the thermodynamically unfavored hexagonal (WZ) instead of the cubic (ZB) phase during the catalyst crystallization of self-catalyzed [Ga]-GaAs NWs is a common occurrence[5] and special procedures must be used to avoid crystal phase mixing.[6] As we could not find any published reference on the crystallization of [Ga]-GaP NWs, we performed our own experiments (Fig. S3). As in [Ga]-GaAs NWs,[5] a typical ZB/WZ/ZB sandwich (Fig. S3.b) is found at the top the [Ga]-GaP NWs, where the Ga catalyst is progressively shrinking as it crystallizes. The particular ZB/WZ/ZB arrangement is associated to the progressive change in contact angle of the Ga catalyst during the crystallization,[7] which impacts the preferred nucleation site: away (ZB) or close (WZ) to the triple phase line.[8]

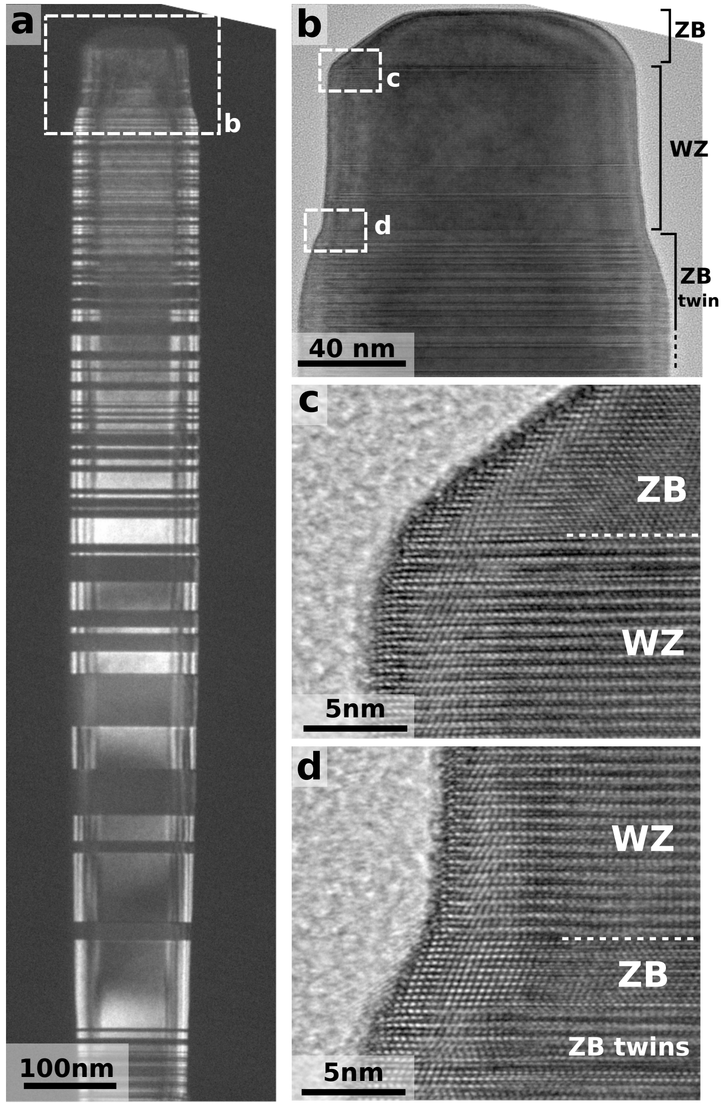

Figure S3: TEM analysis of [Ga]-GaP NWs which catalyst has been crystallized using P flux. (a) Dark field (111) TEM image showing cubic (ZB) twin contrast along the nanowire length. (b) HR-TEM image of the top section of the NW, showing the hexagonal (WZ) segment between two cubic (ZB) segments. (c-d) HR-TEM details of the upper and lower transition zones between the WZ and ZB segments. The change from cubic to hexagonal crystal structure is clearly visible.

The [Ga]-GaP NWs were grown using the same condition than in the main text. The Ga flux is fixed 1.5 Å.s^{-1} (equivalent growth rate on 001 GaAs) and P flux corresponds to atomic V:III ratio of 1.2 as determined by growth rate measurements (RHEED oscillation) using a GaP(100) planar substrate. The substrate temperature is 600 °C and the growth duration is 20 min.

Crystal phase and chemical composition of [In]-(InGa)As nanowires (Ga:In = 1:1)

In this section, we characterize [In]-(InGa)As NWs which catalyst has been consumed using As (Fig. S4). This experiment is similar to to the catalyst consumption of [In]-GaP NWs (see Fig. 5, main text), but applied to a ternary InGaAs solid phase.

These particular [In]-(InGa)As are grown using a substrate temperature of 520°C and a Ga flux of 1.8 Å.s^{-1} equivalent (001) planar GaAs. This Ga flux is slightly higher than that of main text (1.5 Å.s^{-1}). The As/Ga atomic flux ratio is also not 1.4 but 2.0 (higher As flux). The atomic Ga:In flux ratio is still 1:1. The catalyst consumption is performed by exposing the NW to As during 15 min. The same As atomic flux and substrate temperature (520°C) are used than the main growth step (15 min).

Although the Ga:In flux ratio is still 1:1, those [In]-(InGa)As NWs cannot be directly compared to that of the main text (Fig. 2b) due to the higher Ga, In and As fluxes. However we observe similar chemical composition features in the ternary $In_xGa_{1-x}As$ solid, with x the InAs fraction. The top of the NWs is characterized by a high In content, $x \simeq 0.22$, while the base of the NW is In-poor $x \simeq 0.06$ (Fig. S4.e). These values are similar to those of reported in the main text, for the composition of [In]-(InGa)As NWs observed before the catalyst consumption (Fig. 2.d-e, main text).

The variations of the In content are not trivial and may be characterized by two gradients along the axial and radial directions (Fig. S4.e). The radial component is most pronounced in the middle section, with $x = 0.16 \pm 0.01$ when sampling the NW core and $x = 0.12 \pm 0.01$ closer to the NW sidewalls. Such radial gradient can be explained by introducing different In incorporation efficiencies for the axial VLS (core) and radial VS (shell) growth. These two processes operate concurrently so that the NW sidewall remains vertical and flat,[9] but create ternary alloys of different chemical composition due to their separate nature (VLS vs. VS), unless the growth parameters are adjusted specifically.[10] Note that the EDS measurement along the axis of the NW, integrates both the (VLS) core and the (VS) shell compositions (weighted by their respective thickness), while the EDS along the NW edge mostly samples the VS shell composition.

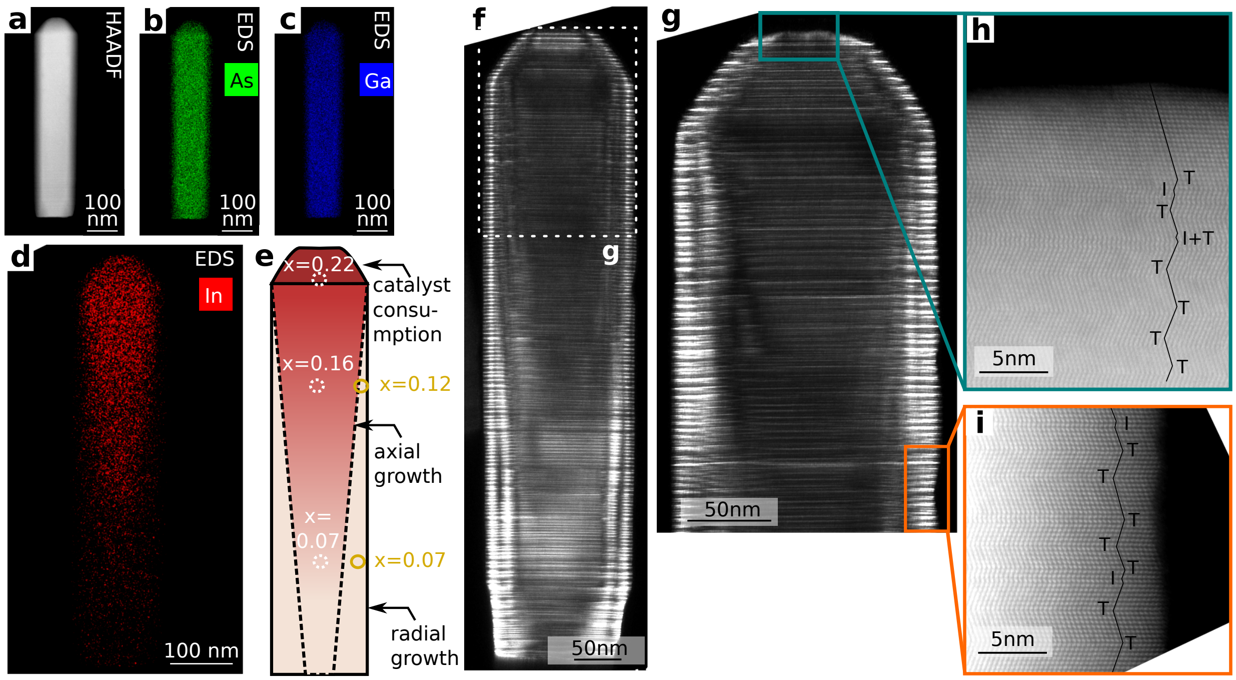

Figure S4: Chemical composition and crystal phase of [In]-(InGa)As NWs which catalyst has been consumed by exposure to a As flux. (a) HAADF image and corresponding As (b), Ga (c) and In (d) elemental maps acquired by EDS. (e) Tentative schematic of the overall growth process, differentiating the radial and axial growth components, as well as the volume created by the consumption of the In catalyst. EDS measurements indicate the InAs fraction x in $In_xGa_{1-x}As$ at selected positions. (f) Dark field TEM (111) image which contrast highlights the local cubic twin orientation. (g) Details of the top section of the NW imaged by dark field TEM. (h) HR-STEM image of the final top layers of the NW. (i) HR-STEM image along the NW main section, far from the catalyst. The atomic structure is always cubic (ZB), the I, T and I+T notations refer to intrinsic stacking fault, twin and their combination, respectively (see Fig. 5 of the main text for more detail).

The axial gradient is more complex and further decomposes into two phenomena.

First, the VS-grown shell is impacted by the different shadowing of the top and the bottom surface of the NW sidewall in our dense hexagonal arrays (pitch 300 nm). It is thus possible that the shell composition differs between the NW top and base, even if they are grown by the same VS process, at constant substrate temperature and nominal fluxes.

Second, the axial VLS-grown core composition can vary during the growth due to changes in the liquid VLS catalyst, as indicated from the thermodynamic analysis (see Fig. 1, main text). At the start of the growth, the initial solid phase crystallizes by VLS process using the pre-deposited [InGa] droplets fabricated with Ga:In=1:1. At this stage, we can expect these initial VLS catalysts to exhibit a significant Ga fraction (see typical droplet size, Fig. 7.c of main text). However the EDS analysis of the main text (Fig. 2.d-e, main text), indicates that the [InGa]-(InGa)As catalysts are nearly pure In after 15 min of growth. Consequently, it is likely that these VLS catalysts evolve from a Ga-rich (early stage) to a Ga-poor composition (steady state) during the growth. Therefore, we can expect the VLS-grown InGaAs core to be Ga-rich (In-poor) at the base and Ga-poor (In-rich) at the top of the NW, which is coherent with our EDS measurements (Fig. S4.e).

Figure S4.f-h reveals that our [InGa]-(InGa)As NWs present a pure cubic phase (ZB), but with a very high density of intrinsic stacking faults (I), cubic twins (T) and their combination (I+T). As explained in the main text, those defects correspond respectively to 1, 2 and 3 monolayers of hexagonal phase (WZ) sandwiched between longer cubic segments.

The absence of WZ phase persists during all the In catalyst consumption, right to the final top layers (Fig. S4.i), where the crystal still exhibits a faulted (and twinned) ZB phase, similarly to the main NW segment (Fig. S4.h).

As these particular [In]-(InGa)As NWs (Fig. S4) present a comparable solid composition than those of the main text (Fig. 2, main text), despite the slight differences in the growth parameters (see above), we can hypothesize that they hold the same pure nearly In catalyst, before its consumption. Under this assumption, the final contact angle of [In](InGa)As NWs is also $\beta_{In}^{InGaAs} \simeq 95°$ (see Fig. 2, main text).

We thus face the same situation than in our (faulted) cubic [In]-GaP NWs (Fig. 5, main text) with $\beta_{In}^{GaP} \simeq 95°$ and we can proceed with the same analysis (section 5 main text, 'Catalyst consumption').

We thus conclude that the use of In catalyst can ensure that [In]-(In_xGa_{1-x})As NWs (x=0.07 - 0.22) remains of the pure (faulted) cubic ZB phase, from the steady growth right to the total catalyst consumption using a As flux.

References

(1) Li, C.; Li, J. B.; Du, Z.; Zhang, W. A thermodynamic assessment of the Ga-In-P system. *Journal of Phase Equilibria* **2000**, *21*, 357–363.

(2) Shen, J.-Y.; Chatillon, C.; Ansara, I.; Watson, A.; Rugg, B.; Chart, T. Optimisation of the thermodynamic and phase diagram data in the ternary As-Ga-In system. *Calphad* **1995**, *19*, 215–226.

(3) Dinsdale, A. SGTE data for pure elements. *Calphad* **1991**, *15*, 317–425.

(4) Ansara, I.; Chatillon, C.; Lukas, H.; Nishizawa, T.; Ohtani, H.; Ishida, K.; Hillert, M.; Sundman, B.; Argent, B.; Watson, A.; Chart, T.; Anderson, T. A binary database for III-V compound semiconductor systems. *Calphad* **1994**, *18*, 177–222.

(5) Kim, Y. H.; Park, D. W.; Lee, S. J. Gallium-droplet behaviors of self-catalyzed GaAs nanowires: a transmission electron microscopy study. *Applied Physics Letters* **2012**, *100*, 033117.

(6) Dastjerdi, M. H. T.; Boulanger, J. P.; Kuyanov, P.; Aagesen, M.; LaPierre, R. R. Methods of Ga droplet consumption for improved GaAs nanowire solar cell efficiency. *Nanotechnology* **2016**, *27*, 475403.

(7) Jacobsson, D.; Panciera, F.; Tersoff, J.; Reuter, M. C.; Lehmann, S.; Hofmann, S.; Dick, K. A.; Ross, F. M. Interface dynamics and crystal phase switching in GaAs nanowires. *Nature* **2016**, *531*, 317–322.

(8) Glas, F.; Harmand, J.-C.; Patriarche, G. Why does wurtzite form in nanowires of III-V zinc blende semiconductors? *Physical Review Letters* **2007**, *99*, 146101.

(9) Oehler, F.; Cattoni, A.; Scaccabarozzi, A.; Patriarche, G.; Glas, F.; Harmand, J.-C. Measuring and modeling the growth dynamics of self-catalyzed GaP nanowire arrays. *Nano Letters* **2018**, *18*, 701–708.

(10) de Lépinau, R.; Scaccabarozzi, A.; Patriarche, G.; Travers, L.; Collin, S.; Cattoni, A.; Oehler, F. Evidence and control of unintentional As-rich shells in GaAs1-xPx nanowires. *Nanotechnology* **2019**, *30*, 294003.